Study on Chloroquine phosphate loading capacity of MIL-100(Fe) synthesized by sonochemical method

Le Thanh Bac[1*], Nguyen Thi Hoai Phuong[1], La Duc Duong[1], Nguyen Thi Phuong[1], Tran Thi Cam Le[2]

[1]Institute of Chemistry and Materials/Academy of Military Science and Technology.
[2] Hanoi National University of Education
*Email: lethanhbac888@gmail.com

ARTICLE INFO

ABSTRACT

Iron-based metal-organic framework (MIL-100(Fe)) was successfully synthesized by sonochemical method at the frequency of 20.5kHz, power of 1080 W in 10 minutes. Several physical measurements were conducted to characterize the MIL-100(Fe) including XRD, FT-IR, Raman, BET, and SEM methods. The analysis results show that the material has characteristic diffraction peaks at 11°, 19°, 24°, and 28°, the specific surface area of the material reaches 1080 m^2/g according to BET, and the particle size from 200-400 nm according to SEM. The chloroquine phosphate loading capacity of MIL-100(Fe) was evaluated according to different adsorption kinetic and isothermal models. The results show that the chloroquine phosphate loading process by material consists of two stages: surface adsorption and intra-particle diffusion. The maximum chloroquine phosphate adsorption capacity of the material reached 236 (mg/g) according to the Langmuir model.

Introduction

Metal-organic frameworks (MOFs) were successfully studied in 1995 by Yaghi et al [1]. Due to their unique characteristics such as large specific surface area, structural flexibility, and adjustable pore size, MOFs have attracted wide attention and their applications have been expanded in many fields such as catalyst [2,3], gas storage [4], drug delivery [5], environmental treatment [6,7].

MIL-100(Fe) is a metal-organic framework with the combination of Fe_3O subunits and organic ligands 1,3,5- benzenetricarboxylic acid. The material has a porous structure with a large surface area (~ 1456.10 m^2/g BET) and pore volume (~1.25 cm^3/g) [4]. This is a potential material for several applications such as gas storage, adsorption, and treatment [8,9]... and MIL-100(Fe) material is also attracted lots of attention in research and application in the field of drug delivery [10]. This material is synthesized from different methods such as sonochemical [11], hydrothermal [12,13], microwave [14], reflux [15], electrochemical method [16]... Hydrothermal is the most frequent method used, however, long synthesis time, high temperature and pressure, which consume a lot of energy are the main disadvantages of this method. Recently, green synthesis methods such as microwave, sonochemical or mechanical have attracted more attention from scientists due to their short synthesis time, good efficiency, and reduced energy consumption [17].

Chloroquine phosphate is commonly used in the treatment and prevention of malaria in the form of pharmaceutical drugs [18] and used to treat other

diseases such as amoebiasis [19] and rheumatoid arthritis as an anti-inflammatory [20]. In 2020, CQp becomes more and more attractive due to its ability to treat diseases caused by COVID-19 [21]. However, when using Chloroquine, it is easy to cause overdose shock due to its low toxicity limit [22]. Therefore, chloroquine is often used in tablet form with the addition of excipients or as an adsorbate.

In this study, we successfully synthesized MIL-100(Fe) by sonochemical method and studied the CQp adsorption capacity of MIL-100(Fe) as a chloroquine phosphate adsorbent.

Experiments and methods

Chemicals and apparatus

Chemicals: $FeCl_3.6H_2O$; 1,3,5-benzenetricarboxylic acid (H_3BTC), chloroquine phosphate, ethanol. Apparatus: drying oven, centrifuge, analytical balance, glassware, sonochemical equipment.

Synthetic process of MIL-100(Fe)

The process of synthesizing MIL-100(Fe) by sonochemical method is shown in Figure 1.

Figure 1: Synthesis process of MIL-100(Fe)

- Mill-100(Fe) was synthesized by sonochemical methods according to the molar ratio $FeCl_3.6H_2O$: 1,3,5 H_3BTC: H_2O of 5,4 (g): 2.8 (g): 200 (ml). Briefly, $FeCl_3.6H_2O$ and distilled water were combined in a PET plastic cup. The solution was stirred until $FeCl_3.6H_2O$ was completely dissolved in water. Then, 1,3,5 H_3BTC was added to the PET plastic cup.

- Ultrasonic device was operated at a fixed probe (Ø) of 15mm in 10 minutes, with a power of 1080W and a frequency of 20.5kHz

- The material obtained after the reaction was filtered and washed 3 times with alcohol and 3 times with distilled water, then dried at 150°C.

Material characterization method

X-ray diffraction (XRD) patterns were analyzed the components of material (X'Pert Pro equipment at Hanoi University of Science and Technology). Textural properties (surface area and pore volume) of Mil-100(Fe) were figured out by N_2 porosimetry (Quantachrome device at Vietnam Academy of Science and Technology). Specific surface areas were evaluated using the Brunauer–Emmett–Teller (BET) equation from N_2 isotherm curves by Scanning electron microscope SEM Hitachi S4800 at the materials laboratory, Vietnam Academy of Science and Technology. The chemical bonds and structure of the materials were evaluated through FPIR (Transform infrared spectroscopy (FT-IR) Perkin Elmer Spectrum 2 at Military Technical Academy) and Raman spectroscopy (Raman Thermo Scientific DXR3 instrument at the Institute of Chemistry and Materials).

Methods to evaluate chloroquine phosphate (CQP) adsorption capacity of MIL-100(Fe)

Evaluation of CQp adsorption rate

Weigh 0.01g of MIL-100 and soak it in 10 ml of 300ppm CQP solution at room temperature (25°C). After different periods, the concentrations of the solutions were measured again to evaluate the adsorption capacity at different periods.

Evaluation of maximum adsorption capacity

Weigh 0.01g of MIL-100 then soaking in 10ml of CQP solution with different concentrations: 200ppm, 300ppm, 400ppm, 500ppm, 800ppm, 1000ppm, 2000ppm at room temperature (25°C). After the saturation adsorption time (14 days), the concentrations of the solutions were measured again to determine the saturation adsorption concentration.

Measuring UV-Vis spectroscopy to determine the concentration of CQP in solution

Based on UV-Vis photometric analysis technique to evaluate the CQP adsorption capacity of materials. The standard curves show the adsorption capacity of CQP in aqueous solvents was built from samples of 10ppm, 20ppm, 30ppm, 40ppm, and 50ppm.

The calibration curve of CQP in water at the wavelength of 329nm was shown in Figure 2:

$$y = 37.387x - 2.2474 \quad\quad (1)$$

Where: y is the concentration of CQP, x is the intensity of adsorption (abs) with correlation coefficient $R^2 = 0.9926$.
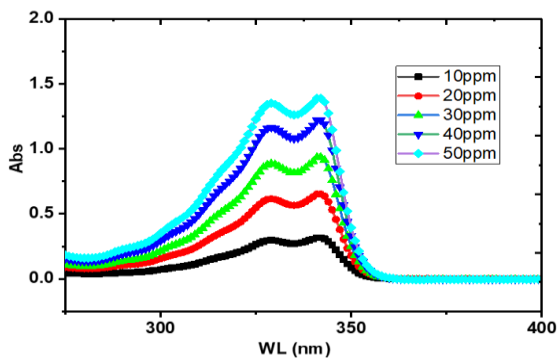

Figure 2: UV-vis spectrum of CQP in water at different concentrations

Results and Discussion

Characteristics of MIL-100(Fe)

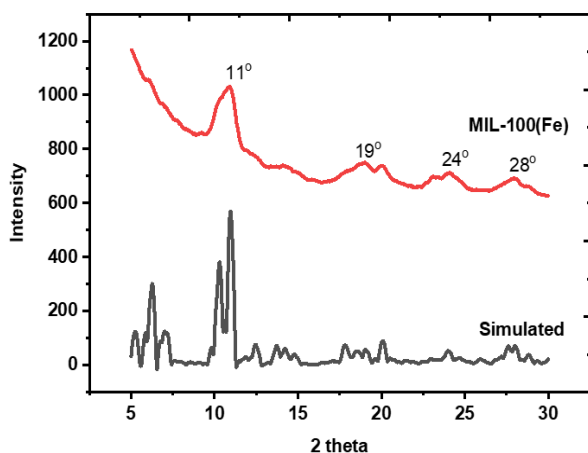Figure 3: The material after drying and fine grinding

Figurs 4: X-ray diffraction spectrum

The material after synthesizing by sonochemical method has the form of a fine brown powder. The crystallinity of the material was investigated by X-ray diffraction (Figure 4). The results show that the obtained materials have characteristic peaks at 11°, 19°, 24°, and 28°, which are similar to those previously reported [23,24]. The height of the peak is low, and the peak width is large because the material is synthesized by sonochemical method, which makes the crystals to be formed quickly. The obtained product has a lower crystallinity than that of the traditional hydrothermal method, so the obtained diffraction peaks are not high. The shape of the MIL-100(Fe) material was observed by scanning electron microscope SEM (Figure 5). The grain size of the material ranges from 200 nm to 400 nm. The small particles are obtained thank to sonochemical synthesis process, which is formed in a short reaction time (less than 10 minutes), and ultrasonic waves are the dispersing agent that hinders the grain growth of the material. However, the material particles tend to agglomerate together into large clumps.
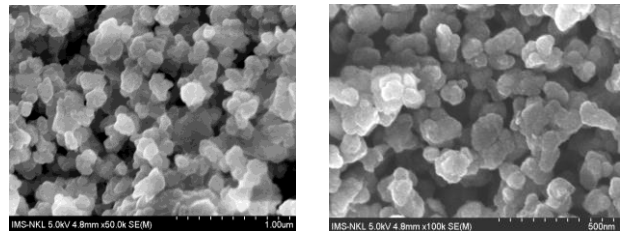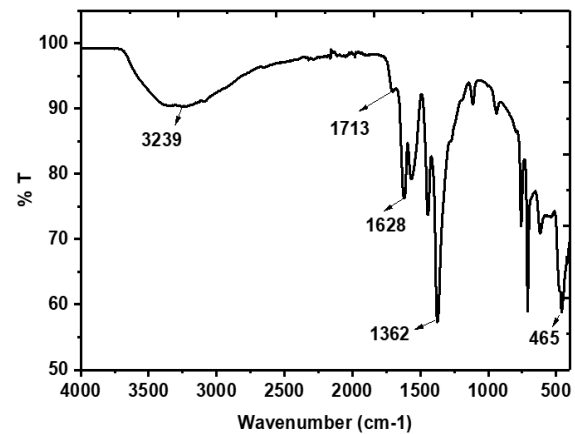

Figure 5: SEM images of MIL-100(Fe)

Figure 6: IR spectrum of MIL-100(Fe)

The chemical bonds and structure of the materials were evaluated through FPIR and Raman spectroscopy. On the FTIR spectrum (Figure 6), the vibration at 3239 cm^{-1} is a stretching O-H vibration in the MOF due to the presence of H_2O in the molecule, vibration at 1713 cm^{-1} is due to -COO stretching vibration in acid H_3BTC, vibration at 1713 cm^{-1} have low intensity due to the small amount of residual H_3BTC acid (due to the washing and filtration process). The vibration at 1628 cm^{-1} and 1362 cm^{-1} are the symmetric and asymmetrical

vibrations of the COO- group, while the vibrations at 465 cm^{-1} correspond to the Fe-O stretching vibrations. These results show that the structure of MOF is formed with organic – trimesic acid and metal ions linkage.

The analysis results on the Raman spectrum shown in Figure 7 also gives similar results. The range from 203 cm^{-1} to 476 cm^{-1} is due to the presence of Fe in the lattice. The bands at 802 cm^{-1} and 1005 cm^{-1} represent the aromatic nucleus vibration relative to the BTC group. The peak observed at 1217 cm^{-1} is due to the C-O-Fe bonding of the iron trimer, and the peaks from 1385 cm^{-1} to 1620 cm^{-1} are related to H-OH bond vibration due to molecular binding water.
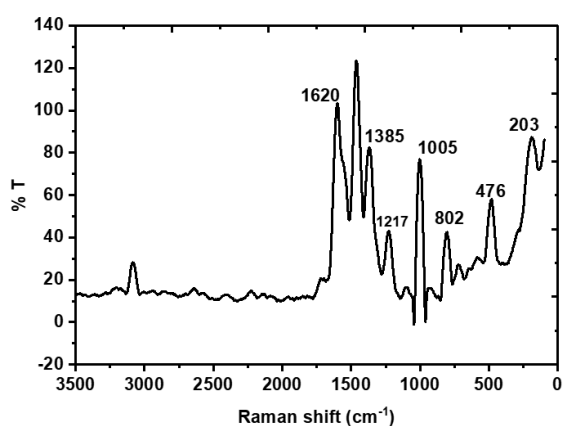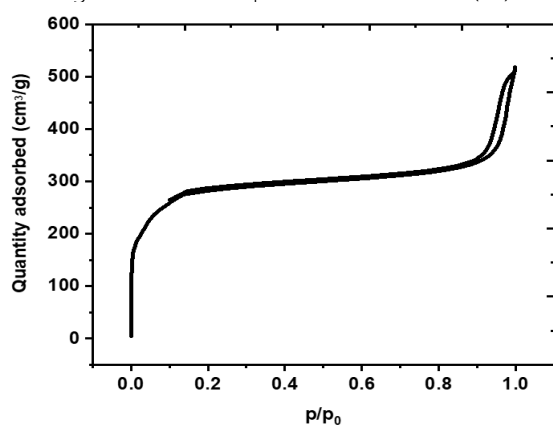

Figure 7: Raman spectrum of MIL-100(Fe)

Figure 8: Nitrogen adsorption isotherm of the material Surface area is another characteristic property of materials. The surface area of the material was evaluated by nitrogen gas isothermal adsorption (Figure 8). The nitrogen adsorption isotherm of the material is type II (according to the IUPAC classification) with a type H3 hysteresis ring typical of mesoporous materials and the presence of a macropore ratio. The evaluation results show that the material has a high surface area (1080 m^2/g according to BET) and has a pore volume and pore diameter of 0.50 cm^3/g and 1.89 nm. This porous nature of the

material is perfectly suited for drug-carrying applications.

Chloroquine phosphate adsorption capacity of MIL-100(Fe)

Materials synthesized by sonochemical method were evaluated for chloroquine phosphate adsorption capacity through adsorption rate and maximum adsorption capacity.

The graph (Figure 9) shows the dependence of the adsorption capacity (Q) on time (t). Figure 9 shows that the material is absorbed rapidly in the first 4 hours (average 10 mg/g.h) and decreases gradually over the next hours until equilibrium is reached. After 48 h of adsorption, the adsorption capacity continued to increase, but the adsorption rate gradually decreased, because the adsorption process gradually reached saturation, and the concentration of active substances in the solution decreased.
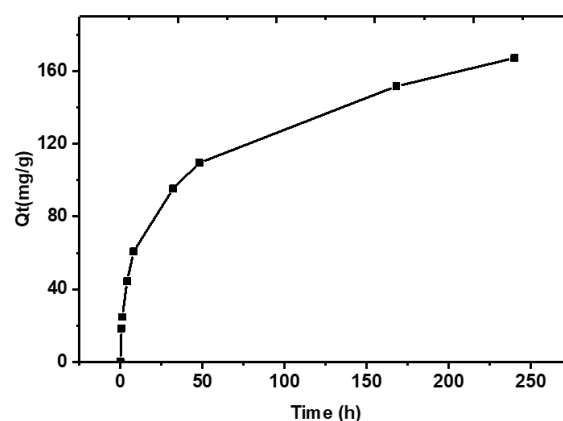

Figure 9: The adsorption capacity (Qt) depends on time t(h)

The adsorption mechanism of the material was evaluated based on the intra-particle diffusion model proposed by Weber and Morris. The absorbate from the external surface of the adsorbent enters inside the capillary to contact the adsorption centers, called the intra-particle diffusion stage. The next stage is the actual adsorption process between the adsorbent and the active sites outside and the capillary inside. The model of intra-particle diffusion is expressed by equation (2):

$$Q_t = K_{id}.t^{0.5} + C \qquad (2)$$

Where: k_{id} (mg.g^{-1} .h$^{-0.5}$) is the intraparticle diffusion rate constant and C represents the boundary layer effect of adsorption.
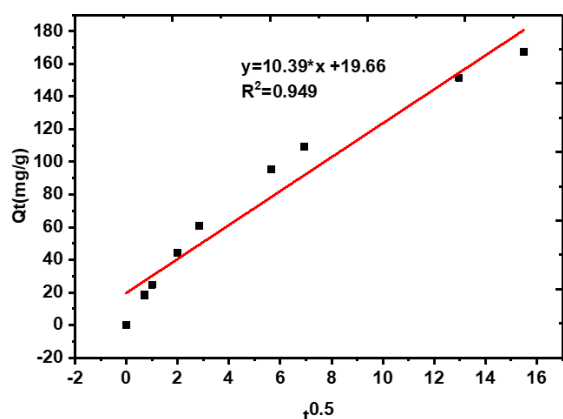
Figure 10: The dependence of the adsorption capacity Q_t on $t^{0.5}$

The equation shows the dependence of the adsorption capacity (Q_t) on $t^{0.5}$ with a large correlation coefficient $R^2 = 0.949$ shows that, Weber and Morris's models are relatively suitable to evaluate the CQP adsorption rate of materials. At the beginning of CQP adsorption (0h-48h), the graph is a steep increase due to adsorption at the external surface adsorption or instantaneous adsorption, the next stage is the diffusion process from the external surface to the internal of the material's structure.

Table 1: CQP adsorption capacity of the material over time

Time (h)	$t^{0.5}$	Q_e (mg/g)
0	0	0
0.5	0.707107	18.39
1	1	24.68
4	2	44.34
8	2.828427	60.72
32	5.656854	95.29
48	6.928203	109.48
168	12.96148	151.62
240	15.49193	167.15

The maximum CQp adsorption capacity of the samples was conducted with different initial CQP concentrations according to isothermal adsorption models. The material after soaking to saturation is filtered to take the solution to conduct UV-Vis measurements. The results are shown in Table 2.

Several adsorption isotherm models have been used to study the adsorption of Chloroquine phosphate in MIL-100(Fe) materials such as Langmuir, Freundlich, and Dubinin - Radushkevich.

Table 2: The maximum adsorption capacity of the material at different concentrations

Sample	C_0 (mg/L)	C_e (mg/L)	Q_e (mg/g)	RL
200 ppm	203.97	65.82	138.15	0.0611
300 ppm	295.64	118.26	177.38	0.0430
400 ppm	424.78	226.78	198.00	0.0303
500 ppm	525.87	323.75	202.12	0.0246
800 ppm	789.88	579.92	209.95	0.0165
1000 ppm	999.19	779.88	219.31	0.01313
2000 ppm	1983.18	1752.23	230.95	0.0066

The Langmuir adsorption assumes that adsorption occurs at specific homogeneous sites within the adsorbent. The Langmuir equation is chosen to estimate the maximum adsorption capacity corresponding to complete monolayer coverage on the homogenous adsorbent surface. Langmuir isotherm equation is expressed by equation (3):

$$\frac{Ce}{Qe} = \frac{1}{Qmax}K + \frac{Ce}{Qmax} \qquad (3)$$

Where:
Q_e (mg/g): Adsorption capacity at equilibrium.
C_e (mg/l): Concentration of adsorbent at equilibrium.
Q_{max} (mg/g): Maximum adsorption capacity.
K (L/mg): Langmuir constant.

In addition, the Langmuir adsorption isotherm is also characterized by the drug adsorption capacity of the material, expressed in terms of separation coefficient (RL) or equilibrium coefficient, expressed by:

$$R_L = \frac{1}{1+K.C_0} \qquad (4)$$

Where: C_0 (mg/g) is the initial concentration of CQp
The separation factor (R_L) indicates the isotherm shape and determines whether adsorption is favorable or not. If $R_L = 0$, adsorption is irreversible; if $0 < R_L < 1$, adsorption is favorable; if $R_L = 1$, adsorption is linear; and if $R_L > 1$, adsorption is unfavorable.

Results according to the Langmuir model show that the material can adsorb CQp with the maximum capacity $Q_{max} = 236.406$ (mg/g) and high correlation coefficient ($R^2 = 0.9996$). These results show that the CQp adsorption process of the material is suitable according to the Langmuir isothermal model. The obtained separation coefficient has a small value (0.0611-0.0066), which shows that the adsorption process is favorable.

Experimental results when the initial concentration at 2000 ppm also showed that the material adsorbed 230

(mg/g), this result is close to the theoretical calculation result. This can also be explained because the drug adsorption process at room temperature is favorable and almost irreversible, so the experimental results can be close to the calculated results.
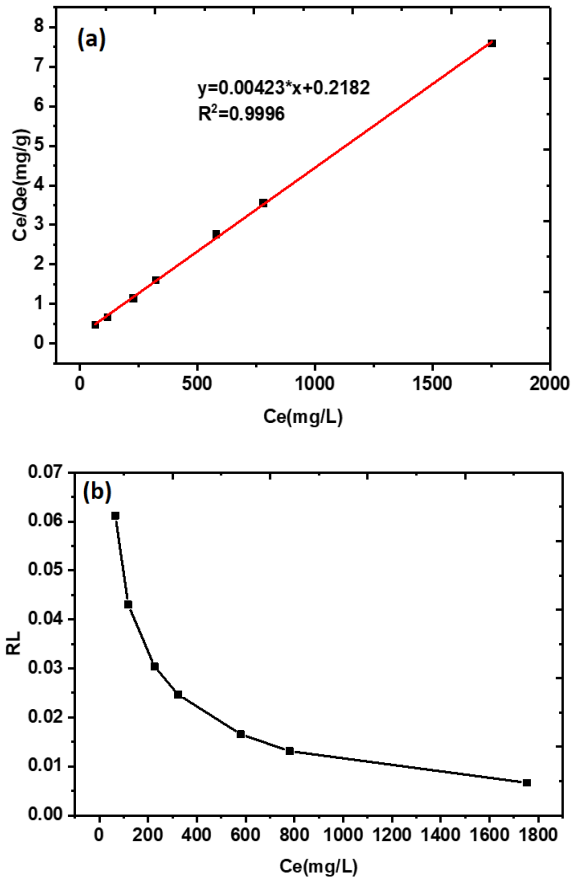

Figure 11: Linear equation of Langmuir isotherm (a) and separation coefficient R_L (b)

The adsorption isotherm according to the Freundlich model is an isotherm adsorption curve based on the assumption of a heterogeneous adsorbent surface. Different from the Langmuir model, the Freundlich model describes the multilayer adsorption and is expressed in equation (5):

$$Q_e = K_F . C_e^{\frac{1}{n}} \qquad (5)$$

The Freundlich isotherm equation in linear form is expressed by equation (6)

$$Ln(Q_e) = \frac{1}{n} . ln(C_e) + \ln(K_F) \qquad (6)$$

Where:

Q_e: adsorption capacity at equilibrium (mg/g).

C_e: concentration of adsorbent at equilibrium (mg/L).

K_F: is Freundlich's constant (mg/g), which is a characteristic quantity for the adsorption capacity of

the system, a large K_F value means a high adsorption capacity.

n: heterogeneity coefficient, is a measure of the heterogeneity of the adsorbent surface and describes the appropriateness of the distribution of adsorbent molecules on the surface of the adsorbent.
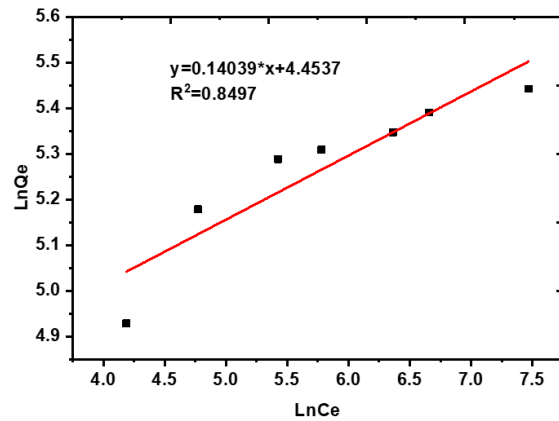

Figure 12: Freundlich isotherm model

The results according to the Freundlich model show that both the Freundlich constant (K_F) and the adsorption strength (n) reach large values (K_F=85,944 and n=7.123). According to the Freundlich model, the correlation coefficient R^2=0.8497 and the heterogeneity coefficient (n) are in the favorable range for the adsorption process. Therefore, the Freundlich adsorption isotherm model is also a relatively suitable model to describe the CQP adsorption process of MIL-100(Fe).

The Dubinin – Radushkevich (D-R) model, based on Polanyi's physical adsorption theory, shows that the adsorption process takes place through physical adsorption or chemical adsorption. The adsorption equation is expressed by equation (7)

$$Ln(Q_e) = \ln(Q_m) - K\varepsilon^2 \qquad (7)$$

Where: Q_m is the maximum adsorption capacity (mg/g), K is the adsorption energy constant (mol^2/J^2), ε is the Polanyi potential, ε expressed as:

$$\varepsilon = RT. \ln\left(1 + \frac{1}{C_e}\right) \qquad (8)$$

Where: C_e is the concentration of the adsorbent retained at equilibrium, R is the ideal gas constant, and T is the temperature (K). The average adsorption energy (E) was calculated according to the equation:

$$E = (2K)^{-0.5} \qquad (9)$$

The average adsorption energy shows whether the adsorption process follows physical adsorption or chemical adsorption:
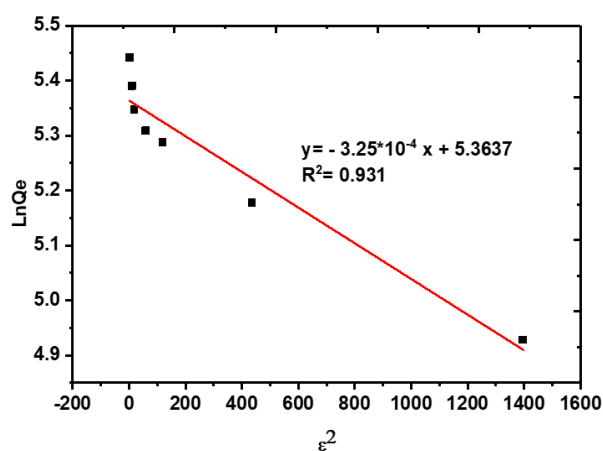

Figure 13. Dubinin-Radushkevich isotherm model

The graph of the Dubinin – Radushkevich (D-R) isotherm is shown in Figure 13. The calculated results according to the D-R model (table 4) show that the maximum adsorption capacity Q_{max} = 213.52 (mg/g) is approximately equal to experimental value. The high correlation coefficient R^2 = 0.931 shows that the Dubinin-Radushkevich model is also suitable to describe the CQp adsorption isotherm process of the material. The high average adsorption energy E = 39.223 (KJ/mol) shows that the adsorption process of CQp into the material is a chemical adsorption process.

Table 3: Summary of isotherm parameters according to Langmuir, Freundlich, and Dubinin-Radushkevich isotherm models

Langmuir	Q_{max} (mg/g)	236.4066
	R^2	0.9996
	K_L	0.0194
	R_L	0.0066 – 0.0611
Freundlich	R^2	0.8497
	K_F	85.944
	n	7.123
Dubinin-Radushkevich	Q_{max} (mg/g)	213.52
	K (mol^2/J^2)	0.000325
	R^2	0.931
	E (KJ/mol)	39.223

Conclusions

MIL-100(Fe) has been successfully synthesized by sonochemical method and applied to efficiently adsorb CQp. The BET evaluation results show that the material has a high surface area (1080 m^2/g) and pore volume, with pore diameters of 0.5 (cm^3/g) and 1.89 (nm), respectively, suitable for drug delivery applications. The CQp loading process of the material can be evaluated through Weber's intra-particle diffusion model. In the first stage, the active substance is quickly adsorbed on the external surface of the material. The next stage is the diffusion process from the external surface to the interior of the material's structure. The CQp loading capacity of the MIL-100(Fe) material was evaluated through the Langmuir, Freundlich, and Dubinin - Radushkevich adsorption isotherm models. The results show that the CQp loading capacity of the material is consistent with the Langmuir model, with correlation coefficient R^2=0.9996 and maximum adsorption capacity reaching 236 (mg/g). With the large maximum CQP adsorption capacity, the MIL-100(Fe) material has the potential to be used as an alternative carrier material for traditional drug adsorbents.

References

1. O.M. Yaghi, G. Li, H. Li, Nature 378 (1995) 703. https://10.1038/378703a0
2. N.M. Mahmoodi, J. Abdi, M. Oveisi, M.A. Asli, M. Vossoughi, Materials Research Bulletin 100 (2018) 357. https://DOI.org/10.1016/j.materresbull.2017.12.033
3. J.J. Delgado-Marín, J. Narciso, E.V. Ramos-Fernández, Materials 15 (2022) 6499. https://DOI.org/10.3390/ma15186499
4. M.A. Simon, E. Anggraeni, F.E. Soetaredjo, S.P. Santoso, W. Irawaty, T.C. Thanh, S.B. Hartono, M. Yuliana, S. Ismadji, Scientific reports 9 (2019) 1. https://10.1038/s41598-019-53436-3
5. A. Mittal, I. Roy, S. Gandhi, (2022). https://10.5772/intechopen.103684
6. A. Yohannes, Y. Su, S. Yao, Metal– Organic Frameworks for Environmental Remediation (2021) 1. https://10.1021/bk-2021-1395.ch001
7. V. Russo, M. Hmoudah, F. Broccoli, M.R. Iesce, O.-S. Jung, M. Di Serio, Frontiers in Chemical Engineering 2 (2020) 581487. https://DOI.org/10.3389/fceng.2020.581487

8. P. Billemont, N. Heymans, P. Normand, G. De Weireld, Adsorption 23 (2017) 225.

9. G. Zhong, D. Liu, J. Zhang, Crystal Growth & Design 18 (2018) 7730.
https://DOI.org/10.1021/acs.cgd.8b01353

10. P.G. Mileo, D.N. Gomes, D.V. Gonçalves, S.M. Lucena, Adsorption 27 (2021) 1123.
https://10.1007/s10450-021-00343-7

11. N.M. Mahmoodi, M. Taghizadeh, A. Taghizadeh, Korean Journal of Chemical Engineering 36 (2019) 287.
https://10.1007/s11814-018-0162-1

12. R. Nivetha, K. Gothandapani, V. Raghavan, G. Jacob, R. Sellappan, P. Bhardwaj, S. Pitchaimuthu, A.N.M. Kannan, S.K. Jeong, A.N. Grace, ACS omega 5 (2020) 18941.
https://doi.org/10.1021/acsomega.0c02171

13. Y. Fang, Z. Yang, H. Li, X. Liu, Environmental Science and Pollution Research 27 (2020) 4703.
https://10.1007/s11356-019-07318-w

14. A. García Márquez, A. Demessence, A.E. Platero-Prats, D. Heurtaux, P. Horcajada, C. Serre, J.S. Chang, G. Férey, V.A. de la Peña-O'Shea, C. Boissière, European Journal of Inorganic Chemistry 2012 (2012) 5165.
https://DOI.org/10.1002/ejic.201200710

15. F. Jeremias, S.K. Henninger, C. Janiak, Dalton transactions 45 (2016) 8637.
https://DOI.org/10.1039/C6DT01179A

16. W.W. Lestari, R. Meilani, I. Nurcahyo, L. Larasati, (2021).
https://DOI.org/10.21203/rs.3.rs-810297/v1

17. S. Kumar, S. Jain, M. Nehra, N. Dilbaghi, G.
https://10.1007/s10450-016-9825-6

Marrazza, K.-H. Kim, Coordination Chemistry Reviews 420 (2020) 213407.
https://DOI.org/10.1016/j.ccr.2020.213407

18. J. Rengelshausen, J. Burhenne, M. Fröhlich, Y. Tayrouz, S.K. Singh, K.-D. Riedel, O. Müller, T. Hoppe-Tichy, W.E. Haefeli, G. Mikus, European journal of clinical pharmacology 60 (2004) 709.
https://10.1007/s00228-004-0818-0

19. C.W. Hart, R.F. Naunton, Archives of Otolaryngology 80 (1964) 407.
https://10.1001/archotol.1964.00750040419009

20. A. Elman, R. Gullberg, E. Nilsson, I. Rendahl, L. Wachtmeister, Scandinavian Journal of Rheumatology 5 (1976) 161.
https://10.3109/03009747609165456

21. M. Huang, M. Li, F. Xiao, P. Pang, J. Liang, T. Tang, S. Liu, B. Chen, J. Shu, Y. You, National Science Review 7 (2020) 1428.
https://10.1093/nsr/nwaa113. eCollection 2020 Sep.

22. A. Della Porta, K. Bornstein, A. Coye, T. Montrief, B. Long, M.A. Parris, The American Journal of Emergency Medicine 38 (2020) 2209.
https://10.1016/j.ajem.2020.07.030

23. H. Lv, H. Zhao, T. Cao, L. Qian, Y. Wang, G. Zhao, Journal of Molecular Catalysis A: Chemical 400 (2015) 81.
https://DOI.org/10.1016/j.molcata.2015.02.007

24. N.E. Elharony, I.E.T. El Sayed, A.G. Al-Sehemi, A.A. Al-Ghamdi, A.S. Abou-Elyazed, Catalysts 11 (2021) 1451.
https://DOI.org/10.3390/catal11121451